Non-Pinned, Reversible Spin Crossover in Self-Assembled Monolayers of a Functionalized Fe(II) Scorpionate Complex

Rebecca Rodrigues de Miranda, Niccolò Giaconi, Margaux Pénicaud, Lisa Biwandu, Thierry Buffeteau, Brunetto Cortigiani, Matteo Mannini, Edwige Otero, Philippe Ohresser, Elizabeth Hillard, et al.

Non-Pinned, Reversible Spin Crossover in Self-Assembled Monolayers of a Functionalized Fe(II) Scorpionate Complex

Rebecca Rodrigues de Miranda, Niccolò Giaconi, Margaux Pénicaud, Lisa Biwandu, Thierry Buffeteau, Brunetto Cortigiani, Matteo Mannini, Edwige Otero, Philippe Ohresser, Elizabeth Hillard, Lorenzo Poggini, Mathieu Gonidec,* Patrick Rosa**

**Corresponding authors. ORCID ID's 0000-0002-1931-5841 (L. Poggini), 0000-0002-0187-1305 (M. Gonidec) and 0000-0001-5670-2624 (P. Rosa)*

Rebecca Rodrigues de Miranda, Margaux Pénicaud, Lisa Biwandu, Elizabeth Hillard, Mathieu Gonidec, Patrick Rosa

Université de Bordeaux, CNRS, Bordeaux INP

ICMCB, UMR 5026, F-33600 Pessac, France

Email: rebecca.rodrigues-de-miranda@icmcb.cnrs.fr, margaux.penicaud@gmail.com, lisabiwandu@gmail.com, elizabeth.hillard@icmcb.cnrs.fr, mathieu.gonidec@icmcb.cnrs.fr, patrick.rosa@icmcb.cnrs.fr

Niccolò Giaconi, Brunetto Cortigiani, Lorenzo Poggini, Matteo Mannini

Department of Chemistry and INSTM Research Unit

University of Florence

V. della Lastruccia 3, 50019 Sesto Fiorentino, Italy

Email: niccolo.giaconi@unifi.it, brunetto.cortigiani@unifi.it, lpoggini@iccom.cnr.it, matteo.mannini@unifi.it

Thierry Buffeteau

Université de Bordeaux, CNRS, Bordeaux INP

ISM, UMR 5255, F-33405 Talence, France

Email: thierry.buffeteau@u-bordeaux.fr

Edwige Otero, Philippe Ohresser

Synchrotron SOLEIL

L'orme des Merisiers

91190 Saint Aubin, France

Email: edwige.otero@synchrotron-soleil.fr, philippe.ohresser@synchrotron-soleil.fr

Keywords: spin crossover, Fe L edge, X-ray absorption spectroscopy, scorpionates, self-assembled monolayers, switchable thin films

The spin crossover (SCO) behaviour of molecules in (sub)monolayers is typically significantly altered from that of the bulk: in particular, the SCO can be quenched by direct contact between the SCO molecules and the substrate, known as pinning, which causes problems for potential device applications. Here, an Fe (II) complex is presented that exhibits fully reversible, non-pinned SCO in self-assembled monolayers (SAMs) on template stripped gold substrates. The complex, [Fe(Tp(4-NHCOC$_{10}$H$_{20}$SCOCH$_3$))(Tp)] where Tp = tris(1*H*-pyrazol-1-yl borohydride), has a broad SCO with a $T_{½}$ of 366 K. The SAMs are uniform and homogeneous, as indicated by Atomic Force Microscopy, and contain the target molecules in a well-oriented layer with the expected thickness for a monolayer of the complex, as revealed by polarization modulation infrared reflection-absorption spectroscopy, time-of-flight secondary ion mass spectrometry and cyclic voltammetry. Variable temperature X-ray photoelectron spectroscopy, as well as X-ray absorption spectroscopy at the Fe $L_{2,3}$ edges, indicates a reversible SCO in the monolayers that is identical to the bulk behaviour.

Non-Pinned, Reversible Spin Crossover in Self-Assembled Monolayers of a Functionalized Fe(II) Scorpionate Complex

Rebecca Rodrigues de Miranda, Niccolò Giaconi, Margaux Pénicaud, Lisa Biwandu, Thierry Buffeteau, Brunetto Cortigiani, Matteo Mannini, Edwige Otero, Philippe Ohresser, Elizabeth Hillard, Lorenzo Poggini, Mathieu Gonidec,* Patrick Rosa**

1. Introduction

Spin crossover (SCO) compounds, a class of switchable molecular materials, are one candidate for the downsizing of devices through molecular electronics.[1,2] Upon application of an external stimulus, these compounds can switch between two distinct states: low spin (LS) and high spin (HS). SCO compounds are interesting for multi-addressable technologies because it is possible to obtain a huge change in properties (structural, optical, magnetic, electronic) by applying one of numerous stimuli (pressure, heat, light, magnetic and electric fields, chemical environment).[3] This diversity in 'outputs' and 'inputs' gives SCO compounds wide-ranging applications, from chemical sensors to memory devices.[1,2,4] Iron (II) compounds with appropriate ligand field strengths (typically from multi-dentate, nitrogen-coordinating ligands) can exhibit SCO around room temperature and are widely studied for this reason. These octahedral complexes have LS and HS configurations of t_{2g}^6 and $t_{2g}^4{}_{eg}^2$ respectively: The Fe (II) LS state is fully diamagnetic while the HS is paramagnetic.

The fabrication of thin films and monolayers is one approach to decreasing the size of device components. Thin films also help us study what happens at the molecule-substrate interface, and thereby allow for fine control of the film properties[5] if the interface is well understood. In particular, films on metal surfaces are interesting, as the metal can function as a conducting electrode for potential device fabrication. However, incorporation of SCO compounds in devices is complicated by the fact that fabricating uniform films over large (micrometre) areas, in particular through sublimation, is challenging[6–8] as the molecules may dissociate on the surface[9,10] or form islands or nano/micro-crystallites[11,12] rather than a homogeneous layer. Self-assembled monolayers (SAMs) offer a way to prepare ultra-thin films with uniform and homogeneous surface coverage in a chemically controlled way.[13] SAMs can be prepared on metal electrodes, which is a prerequisite for the development of molecular electronic devices.

However, monolayer deposits of SCOs can present an altered behaviour, and so an important consideration when preparing (sub)monolayers of SCO complexes is the potential change in SCO properties at the interface. While in thick films (a few to hundreds of nm) the SCO is unchanged when comparing the film and the bulk,[14,15] in ultra-thin films, strong interactions with the substrate may cause the SCOs to fragment on the surface, or alter the SCO behaviour.[16] In some cases, characterized by scanning tunnelling microscopy (STM), LS and HS states coexist at temperatures far from the transition, and the spin state composition of the film is temperature-independent.[11,17–19]In other cases, where the SCO is characterized by X-ray absorption spectroscopy (XAS), a similar suppression of SCO for molecules in the first layer is observed.[9,10,20,21]

Reports of SAMs of SCO compounds are scarce, with very few examples in published literature. Devid *et. al.* prepared arrays of gold nanoparticles with Fe (II) SCO molecules grafted through a SAM approach, and observed a SCO that was incomplete compared to the bulk.[22] Karuppannan *et. al.* reported physisorbed monolayers of an Fe (III) SCO complex that assembled through iodine-graphene interactions, that retained

their bulk properties due to the SCO molecules being physically separated from the copper substrate by counteranions and a graphene layer.[8] Garcia-Lopez *et. al.* reported a Co (II) complex that assembled through covalent carboxylate-silver interactions, but that exhibited only a partial SCO while a fraction of molecules appeared to be blocked.[23] Attempts to prepare SAMs of SCO molecules through on-surface synthesis - by initially forming a SAM of one of the ligands and later adding the rest of the molecule - have been met with limited success. Even when the ligands form high quality SAMs, it has proven challenging to get the metal centre to bind to the ligand once it is on the surface.[24,25]

Concerning Fe (II) SCO complexes on noble metal surfaces, there are several reports of monolayer or ultra-thin film assemblies: as islands on a Au(111) surface,[26] as two-dimensional assemblies on Au(111), Ag(111) and Cu(111),[27] as (sub)monolayers on Cu(111),[28] or as ultra-thin films on Cu(111).[29] In each of these cases, the metal-molecule interface alters the SCO in the film, and it is different from that of the bulk. In certain cases, the complex degrades during deposition or under X-rays, resulting in Fe (III) and a complete absence of SCO.[30,31]

Here we show that it is possible to prepare homogeneous SAMs of Fe (II) SCO complexes that exhibit a temperature-induced switching that is 1) reversible and 2) identical to the behaviour of the bulk compound. Characterization by time-of-flight secondary ion mass spectrometry (ToF-SIMS), X-ray photoelectron spectroscopy (XPS) and atomic force microscopy (AFM) indicate that the SAMs contain the target complex, and are uniform and homogeneous. Polarization modulation infrared reflection-absorption spectroscopy (PM-IRRAS) in combination with simulations reveals a well-oriented layer with the expected thickness for a monolayer of the complex. Cyclic voltammetry (CV) shows behaviour consistent with a monolayer with good packing. DFT calculations corroborate these results. Variable temperature XPS, as well as X-ray absorption spectroscopy (XAS) at the Fe $L_{2,3}$ edges, indicates a reversible SCO in the monolayers that corresponds closely to the bulk behaviour. The use of multiple techniques to characterise the SCO, in addition to several others to confirm the quality of the SAMs, provides a strong argument for the validity of our conclusions[22] and the resultant applicability of our system in molecular electronics.

2. Synthesis and Bulk Characterization

We chose [$FeTp_2$], where Tp = tris(1*H*-pyrazol-1-yl borohydride), as our parent SCO moiety because it is charge neutral and solution stable (both important properties for preparing SAMs) and because we have good references for its bulk properties. Furthermore, it has recently been shown that it is relatively easy to prepare functionalizable 'building blocks' based on this moiety.[32]

In order to avoid direct contact between the SCO moiety and the metal substrates, we functionalized the molecule with an alkyl spacer, to obtain [Fe(Tp(4-$NHCOC_{10}H_{20}SCOCH_3$))(Tp)] (**Figure 1**), which from here on is referred to as **$FeTp_2$-C11-SAc** (for the bulk) and **$FeTp_2$-C11-S** (in SAMs). The spacer is terminated by a sulphur-based anchoring group so that the molecules can chemically graft to the substrates to form SAMs. The length of the spacer was chosen somewhat arbitrarily, considering that long alkyl chains with a number of carbons $N_C > 15$ can fold and cause packing defects in SAMs, whilst a $N_C < 8$ may increase the frequency of short-able holes in the monolayer, at least in SAMs of alkanethiols terminated by a bulky head group.[33–35]

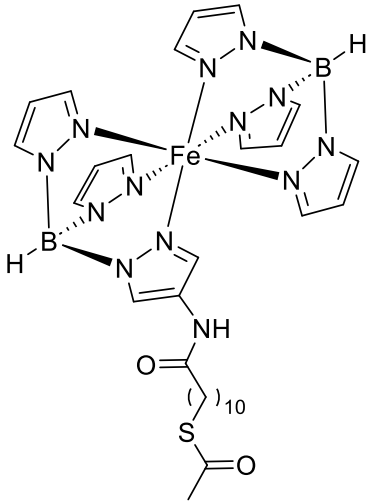

Figure 1 The target molecule [Fe(Tp(4-NHCOC$_{10}$H$_{20}$SCOCH$_3$))(Tp)]. It consists of an [FeTp$_2$] SCO moiety with a 10-methylene spacer and thioacetate anchoring group.

Starting from the Tp and Tp-4-NO_2 ligands, we followed the synthesis described by Flötotto *et. al.*[32] to obtain a mixture of the [Fe(Tp-4-NH_2)(Tp)] and [Fe(Tp-4-NH_2)$_2$] complexes, along with [FeTp$_2$]. To prepare the alkylthioacetate linker, we followed a procedure described by Jaber *et. al.*[36] to synthesize the 11-acetylthoiundecanoic acid, which we then coupled to the amine-functionalized complex via an amidation reaction. The resulting mono-, bis- and non-functionalized complexes were separated by size exclusion chromatography. A final purification by silica gel column chromatography yielded the target molecule at a relatively low overall yield of 15%. In MTp$_2$–type compounds, the symmetric, homoleptic forms are deemed 'highly stable'[37] and their formation is therefore expected to be 'significantly favoured;'[38] the homoleptic forms are thermodynamic products, whereas the heteroleptic forms are kinetic products.[39] A greater reaction yield of the mono-substituted, heteroleptic complex can be attained by using non-stoichiometric conditions[38] or by adding the two ligands in different reaction steps.[40] A detailed description of the synthesis and chemical characterization is given in the Experimental section.

The bulk SCO behaviour was characterized by vibrating sample magnetometry (VSM), which revealed that **FeTp$_2$-C11-SAc** undergoes a gradual SCO with a $T_{½}$ of 366 K (full description accompanying **Supporting Information Figure S1**), comparable to the behaviour reported by the Besson group for the [FeTp$_2$-4-NO_2] building block and their series of bis-functionalized complexes.[32] The magnetic behaviour of **FeTp$_2$-C11-SAc** also closely resembles that of the monoclinic crystalline form of the parent [FeTp$_2$] complex.[41–43] The $\chi_M T$ product is very close to zero below 200 K at 5×10^{-7} m^3 K mol^{-1}, indicating an essentially diamagnetic (LS) state. At 450 K, the maximum measured temperature, we find a $\chi_M T$ value of 33.0×10^{-6} m^3 K mol^{-1}, which is slightly lower than the 37.7×10^{-6} m^3 K mol^{-1} spin-only value expected for a fully HS Fe (II) complex, indicating that the SCO is incomplete at this temperature.

3. Monolayer Preparation and Characterization

3.1 Preparation of SAMs and Surface Chemical Characterization

Monolayers of **FeTp$_2$-C11-S** were prepared on atomically smooth, template stripped[44] gold substrates (Au^{TS}). The preparation of the substrates and the SAMs is described in the experimental section. AFM (**Supporting Information Figure S2**) revealed that the SAMs are homogeneous and marginally rougher than the bare substrate imaged under the same conditions. The overall topology is smooth in both cases, but it is clear from the phase response that the surfaces are distinct. The RMS roughness of the SAM is 7.1 Å, compared to 6.9 Å for the Au^{TS}. There are some defects and small particles on the surface of the SAMs. These can be mitigated by preparing the TS substrates and SAMs in a clean room instead of on a laboratory worktop. Overall, the SAM coverage is smooth and homogeneous.

The presence of **FeTp$_2$-C11-S** in the SAMs was confirmed by ToF-SIMS. The molecular peak and various fragments, unambiguously identified through the isotropic distributions, are homogeneously distributed over the substrate (**Supporting Information Figure S3**).

XPS further confirmed the presence of **FeTp$_2$-C11-S** in the SAMs. The characteristic signals of the relevant elements are present, and semi-quantitative analysis (full description accompanying **Supporting Information Figure S4**) corresponds to the expected elemental ratios. The single peak at 400.1 eV in the N*1s* region can be attributed to the nitrogen atoms on the pyrazole rings.[45] The S*2p* region contains a double feature: one with the S$2p_{3/2}$ and S$2p_{1/2}$ components at 162.0 and 163.2 eV respectively, and the other with these components at 163.8 and 165.0 eV. The lower binding energy feature is assigned to sulphur bound to the gold,[46,47] and the higher energy feature is assigned to unbound, chemisorbed sulphur.[46] The Fe*2p* region is split into five components for each of the *2p* features, and will be further discussed in Section 4.1. Overall, the element-specific spectra are consistent with the presence of **FeTp$_2$-C11-S** in the expected elemental ratios: S/Fe = 1.3 (theoretical 1.0), S/N = 0.1 (theoretical 0.08), Fe/N = 0.1 (theoretical 0.08).

We further confirmed the integrity of the SAMs by PM-IRRAS (**Figure 2**). Comparison between the spectra of the bulk (ATR-FTIR spectroscopy on a dropcast film, in blue) and monolayer (PM-IRRAS, in red) indicates that the molecule remains intact in the monolayers. The spectra closely resemble one another: the bands at 2920 cm^{-1} and 2850 cm^{-1} are assigned to the asymmetric [$\nu_{as}(CH_2)$] and symmetric [$\nu_s(CH_2)$] stretching modes of the methylene groups. These are respectively 3 cm^{-1} and 1 cm^{-1} higher than for a well-oriented (all-trans orientation of alkyl chains) octadecanethiolate SAM,[48] suggesting some disorder in the form of gauche defects.[49] A smaller shift for ν_s versus ν_{as} has also been observed in other, comparable systems.[49,50] The band at 2475 cm^{-1} is assigned to the B-H stretch. The bands related to the amide A (stretching N-H at 3285 cm^{-1}) and the amide I (stretching C=O at 1652 cm^{-1}) modes are not visible on the PM-IRRAS spectrum, contrary to the amide II band (bending C-N-H and stretching C-N at 1549 and 1590 cm^{-1}). Due to the surface selection rule of PM-IRRAS (transition moments oriented parallel to the surface are not visible), we can deduce that the C=O and N-H bonds are nearly parallel to the surface, as expected for well-oriented SAMs. The band at 1689 cm^{-1}, assigned to the C=O stretching mode of the thioacetate group, is observable with a weak intensity on the PM-IRRAS spectrum of the SAM. It is unlikely that the thioacetate group binds to the Au^{TS} by physisorption, given the relatively long incubation time and presence of reactive thiol bonds in solution. Furthermore, the binding mode would have to be significantly tilted, since the C=O would not appear in the spectrum were it parallel to the substrate. Given the good ordering of the alkyl chains, based on the positions of the $\nu_{as}(CH_2)$ and $\nu_s(CH_2)$ modes, this scenario is unlikely. It therefore seems possible that a small fraction of the molecules insert into the SAM upside down, with the FeTp$_2$ moiety towards the substrate. At lower wavenumbers, in the 1500 – 900 cm^{-1} spectral range, we find the different bands of pyrazole groups, with non-preferential orientation due to the isotropic distribution of the six entities in the complex. Overall, the PM-IRRAS spectrum is consistent with a thickness of about 20 Å, as predicted by simulations of a compact, isotropic layer of **FeTp$_2$-C11-SAc** (full details accompanying **Supporting Information Figure S5a**). This is the expected thickness for a single layer of these molecules, and is therefore a strong indication that we indeed form a monolayer.

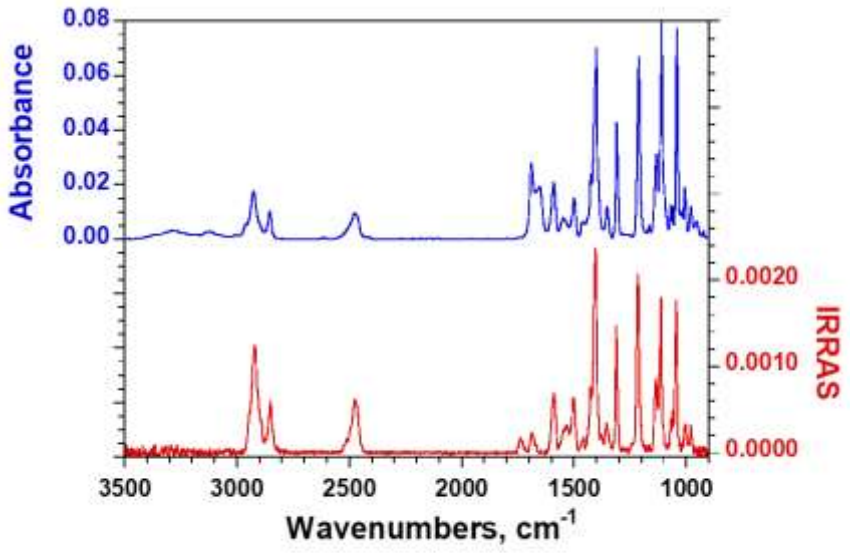

Figure 2 Bulk IR absorption spectrum of **FeTp$_2$-C11-SAc** (blue) and IRRAS on a SAM of **FeTp$_2$-C11-S** on gold (red).

3.2 Electrochemistry

We determined the surface coverage of the SAMs of **FeTp$_2$-C11-S** on gold by CV, referenced to ferrocene (THF – 0.1 M NBu_4PF_6, scan rate 0.05 V s^{-1}) (**Figure 3**). The system was composed of a Pt counter electrode, a Ag/AgCl pseudo reference electrode and a Au working electrode. In SAMs, where molecules are confined to the surface and charge transfer is not diffusion-limited, the oxidation and reduction peaks are expected to appear at the same potential, assuming that the process is fully reversible. The observed CV indeed supports a fully reversible redox process, where the oxidation and reduction peaks appear at -0.16 and -0.19 V, respectively. The shift between the peaks, as well as their slight asymmetry, can be an indication of slow charge transfer kinetics.[51] The half-cell potential is -0.18 V with respect to the ferrocene Fc/Fc^+ redox couple, the same as for bulk **FeTp$_2$-C11-SAc** (**Supporting Information Figure S6**). Ideal peaks have a full-width half maximum (FWHM) described by Equation (1), which in our case, for a temperature of 28°C, predicts a FWHM of 91.5 mV. The experimental FWHM are 107 and 139 mV for the oxidation and reduction peaks, respectively.

$$\text{FWHM (V)} = 3.53\ RT/Fn \quad [52,53] \qquad \text{Equation (1)}$$

Where $R = 8.314$ J K^{-1} mol^{-1} is the molar gas constant, T is the temperature in Kelvin, $F = 9.649\times10^4$ C mol^{-1} is the Faraday constant and n is the number of electrons involved in the redox process, which in this case is shown to be one by comparison with the ferrocene redox process.

Peak widening and asymmetry occur when molecules in the SAM have slightly different energies. Inhomogeneity in molecular energies can happen when molecules occupy different microenvironments, for example when there are SAM defects leading to there being higher and lower energy sites on the surface,[54] or when electron exchange occurs between molecules, in particular in densely packed SAMs.[54] The peak broadening in the CV is consistent with the indication from PM-IRRAS that molecules may insert into the SAM at different orientations.

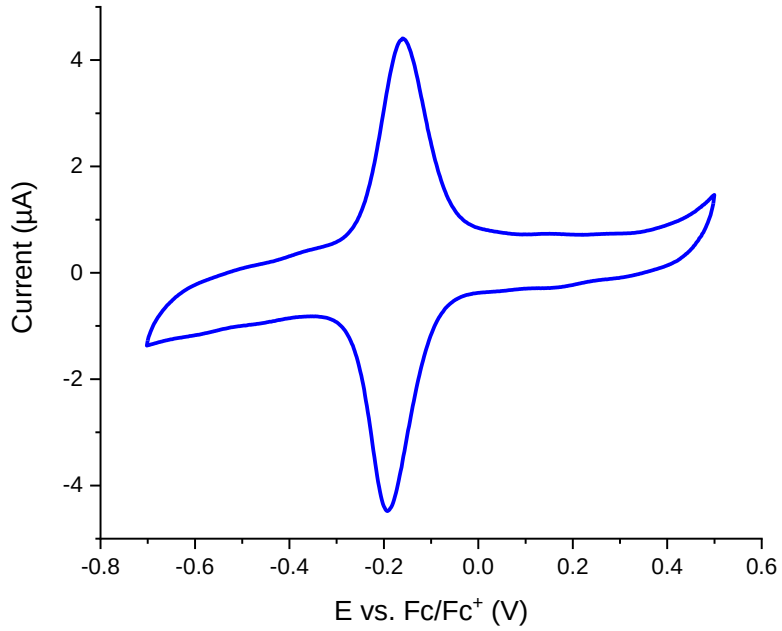

Figure 3 Cyclic voltammogram of a SAM of **FeTp$_2$-C11-S** on Au^{TS} in a solution of THF – 0.1 M NBu_4PF_6 measured at a scan rate of 0.05 V s^{-1}.

By integrating the oxidation and reduction peaks, and disregarding the capacitive background contribution, we can estimate the SAM density using Equation (2) to obtain a surface coverage of ~1.06×10^{14} molecules per cm^2, corresponding to an occupied area of 0.94 nm^2 per molecule.

Γ (mol cm^{-2}) = Q/nFA [55,56] Equation (2)

Where Γ is the surface coverage in mol cm^{-2}, Q is the integrated peak area in C, A is the surface area of the electrode in cm^2, and F and n are as in Equation (1).

Assuming a hexagonal packing of the head groups in the SAM, we obtain a spherical diameter of 1.04 nm per head group. This value corresponds to a dense, organized SAM of **FeTp$_2$-C11-S**. This conclusion is consistent with the geometry of the molecules as estimated by gas phase DFT calculations, which predict a cross section of *ca.* 0.91 nm^2 for the SCO head group of **FeTp$_2$-C11-S**.

4. SCO in SAMs

4.1 X-ray Photoelectron Spectroscopy

The SCO in SAMs of **FeTp$_2$-C11-S** was initially studied by variable temperature XPS in the Fe*2p* region. **Figure 4 (left)** shows the evolution of the spectra with temperature. The spectral changes with temperature indicate a SCO behaviour that is typical of Fe (II) in similar (pseudo)octahedral geometries[6,21,24,31,57–60] and that is qualitatively similar to that of bulk **FeTp$_2$-C11-SAc**. The Fe$2p_{3/2}$ and $2p_{1/2}$ features were fit with five components. The components shaded in blue, labelled *A* for the Fe$2p_{3/2}$ feature (708.3 eV) and *A'* for the Fe $2p_{1/2}$ one (720.9 eV), are indicative of the proportion of LS Fe (II) in the sample: the decrease in the total area of this pair is consistent with a decrease in the LS fraction in the SAMs with increasing temperature. The binding energy increases marginally with temperature, which is characteristic of an Fe (II) sample going

from LS to HS.[61] The shift in binding energy arises because the Fe-N bonds in the HS state are longer: a lower electron density on the iron decreases the energy of the Fe electrons and increases their effective binding energy.[57] The spin-orbit splitting between the *A* and *A'* features increases with temperature, which is again characteristic of a conversion from LS to HS,[60] and is due to the lower population of the e_g-like orbitals at lower temperatures, where the molecules exist mostly in the LS state.[31] The satellites that appear at higher temperatures are characteristic of the iron in its HS state,[61,62] and arise due to the presence of unpaired electrons[63] in the paramagnetic state, as well as the resultant metal-to-ligand charge transfer.[24] Temperature cycling indicates that the SCO is reversible in the range of 160 to 390 K (**Figure 4 right**). Quantitative XPS analysis on monolayer films can be unreliable due to the low intensity of the signals,[31] so we performed a quantitative analysis of the SCO in the SAMs using a more sensitive technique: X-ray absorption spectroscopy.

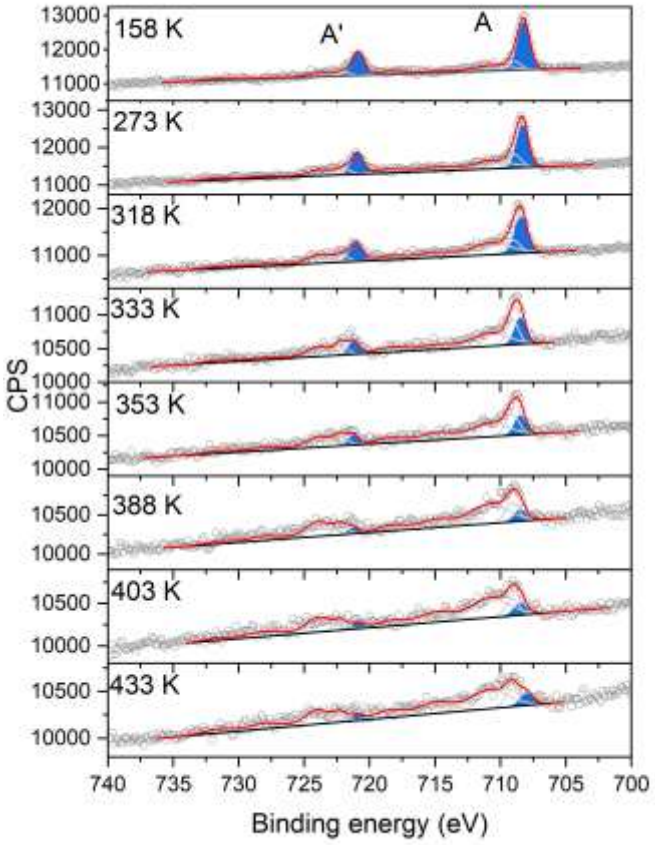

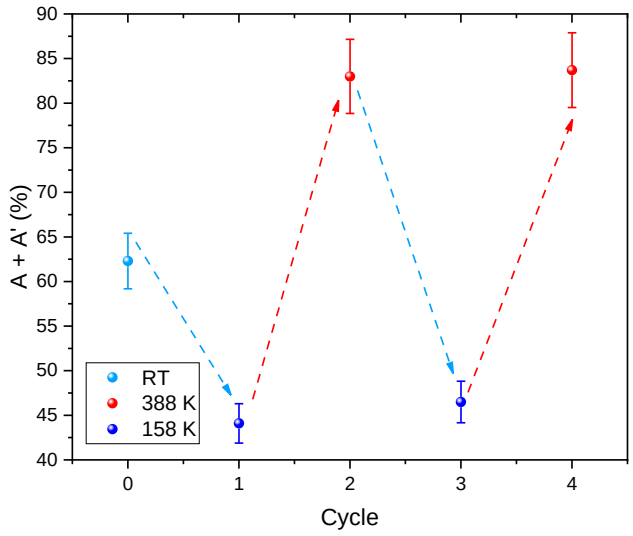

Figure 4 Variable temperature XPS in the Fe*2p* region on a SAM of **FeTp$_2$-C11-S** on Au (left), and the relative (%) area of the shaded pair of peaks, indicative of LS Fe (II) and labelled *A* and *A'*, with cycling between 158 and 388 K (right). The areas do not change with cycling, indicating that the SCO in the SAMs is reversible and that there is no sample degradation.

4.2 X-ray Absorption Spectroscopy

The SCO in monolayers of **FeTp$_2$-C11-S** was quantitatively characterized by XAS at the Fe $L_{2,3}$ edges (**Figure 5**), in total electron yield (TEY) mode. The spectral shapes observed at 4 and 100 K for the isotropic spectra are characteristic of LS Fe (II) compounds with (pseudo)octahedral nitrogen ligand coordination.[6,7,20,21,64–66,59,60] The evolution of the spectra with temperature supports the occurrence of thermal SCO. With increasing temperature, the L_2 and L_3 white lines both decrease in intensity and shift towards lower energies, with a peak at 711.3 eV characteristic of the HS state that begins to emerge at the L_3 edge, and an L_2 edge structure that becomes more complex with a shoulder appearing at 722.5 eV. The excellent signal-to-noise ratio at the DEIMOS beamline allowed us to observe a broad absorption between 716.8 and 721.5 eV that gradually disappears with increasing temperature. This absorption, which we previously observed in another, closely related compound,[21] can be linked to a transition from the Fe*2p* orbital to a final state corresponding to some hybridization with the ligands, as previously reported for Ni (II) complexes.[67] This absorption feature appears to be characteristic of LS Fe (II), which shows stronger hybridization with the ligands, and disappears for HS Fe (II).

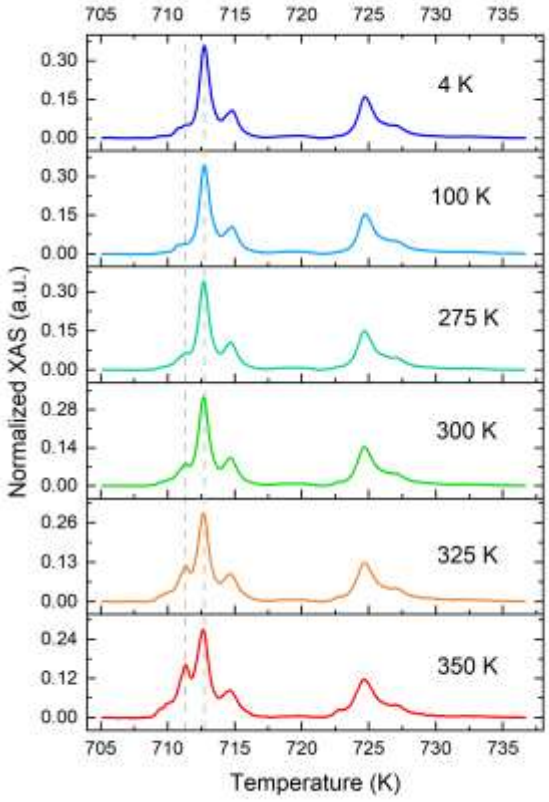

Figure 5 Evolution of the Fe $L_{2,3}$ edge XAS spectra with temperature on a SAM of **FeTp$_2$-C11-S** on Au^{TS}. The dashed grey lines mark the positions of characteristic features for HS and LS Fe (II) at the L_3 edge.

In order to extract a HS fraction at each temperature, the spectra of the SAMs can be decomposed into a linear combination of LS and HS spectral shapes. Typically, this decomposition requires a reference spectrum on the sample in the fully LS state and another in the fully HS state. Due to the high $T_{½}$ of **FeTp$_2$-C11-SAc**, it was not possible to obtain a fully HS spectrum at this particular beamline. For the LS reference, we used the spectra measured at 100 K. The HS reference then was obtained by subtracting the LS spectrum from the spectrum at 350 K. The resulting LS and HS spectral shapes (full description accompanying **Supporting Information Figure S7a**) are in good agreement with those obtained through ligand field multiplet calculations for octahedral Fe (II) that we have reported previously.[20] The symmetry of the first coordination sphere of the parent complex [FeTp$_2$] and other similar Fe (II) compounds is close to perfectly octahedral in the LS state,[20] and **FeTp$_2$-C11-SAc** is expected to follow this trend. The spectra measured on the SAMs follow the same evolution as those measured on a dropcast (bulk) sample(**Supporting Information Figure S7b**). Given that the SAM and bulk samples exhibit the same SCO behaviour, and that our SAM spectra are similar to those of comparable Fe (II) complexes in bulk[6,7,20,21,64–66,59,60] and calculations,[20] we consider it acceptable to use the measurements on the SAMs to obtain the HS and LS references.

The HS fraction n_{HS} was obtained by fitting each spectrum as a linear combination of the LS and HS references (**Supporting Information Figure S7c**). The resulting calculated n_{HS} is plotted in **Figure 6**, together with the n_{HS} extracted from the magnetometric measurements on bulk **FeTp$_2$-C11-SAc**. The XAS measurements reveal a SCO in the SAMs corresponding closely to that of the bulk. We therefore conclude that our SAMs exhibit a SCO that is completely decoupled from the substrate. SCO in (sub)monolayer films is typically significantly altered by the interaction between SCO molecules and metallic, non-magnetic surfaces.[8–11,17–21,23,27–29] It is significant that in our case, designing a complex with a decoupling linker allowed us to observe a rare case of non-pinned SCO in monolayers on metal substrates.

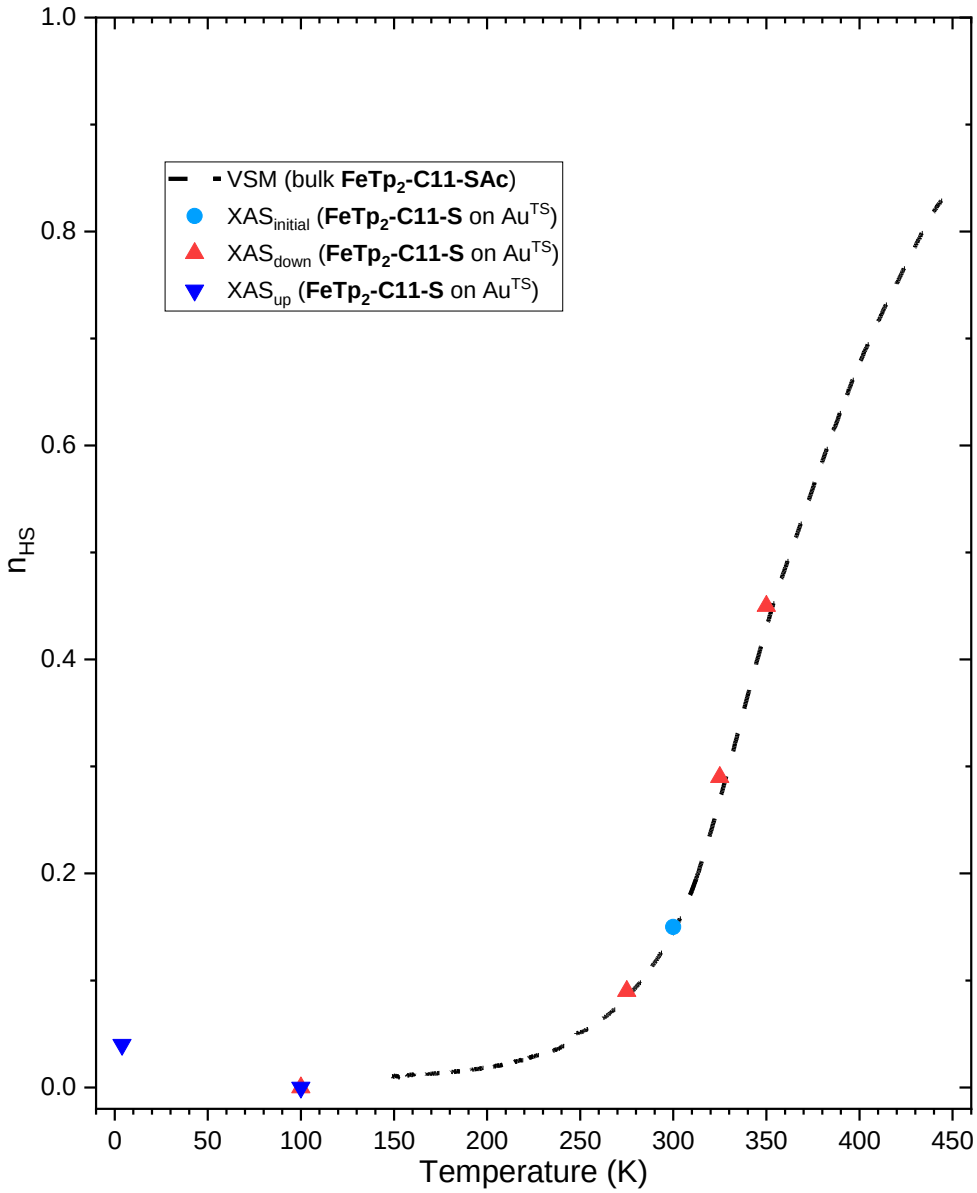

Figure 6 The high spin fraction n_{HS} vs. temperature in SAMs of **FeTp$_2$-C11-S** on Au^{TS} as measured by XAS (solid shapes), overlaid over the curve derived from magnetometric VSM results for the bulk **FeTp$_2$-C11-SAc** (black dotted curve). The light blue circle represents the initial measurement, while the red and blue triangles indicate a measurement performed upon increasing or decreasing the temperature, respectively. The SCO in SAMs is reversible and closely follows the bulk behaviour.

The SCO in the SAMs is reversible and there is no indication of beam damage to the sample. The branching ratio[68,69] is defined as $I_3/(I_3+I_2)$, where I is the integrated area for the corresponding L_2 or L_3 edge. It is expected to increase with increasing HS fraction,[20] and indeed we find a branching ratio of 0.58 at 100 K versus 0.66 at 350 K in the SAM. All of the data points lie along the bulk VSM curve. We therefore conclude that the SCO process in the SAMs is fully reversible, and that there is no beam-induced degradation. The appearance at 4 K of the HS L_3 peak at 711.3 eV may indicate some soft X-ray induced excited spin state trapping (SOXIESST): the fitted spectrum corresponds to a n_{HS} of 0.04, and the branching ratio is 0.61. Given the high $T_{½}$ and the feeble SOXIESST, we did not further explore the light induced excited spin state trapping (LIESST) effect in this complex. The edge jump, calculated by the difference in intensity between the L_3 peak and the pre-L_3 edge baseline, is 0.11 at 100 K. Assuming a TEY probing depth of 5 nm,[70] and using the edge jump of 0.28 measured at 100 K in the dropcast as representative of the bulk, we calculate a film thickness of 1.9 nm, corresponding to the expected thickness of a densely packed, oriented SAM of **FeTp$_2$-C11-S** and in excellent agreement with the PM-IRRAS calculations.

Overall, decomposition of the spectra into the relative LS and HS components, made possible thanks to the high signal-to-noise ratio at the DEIMOS beamline, reveals that the SCO in the SAMs is unaltered from that of the bulk complex.

5. Conclusion

We have designed an Fe (II) complex that exhibits reversible, non-quenched SCO in SAMs on template stripped gold substrates. The complex, [Fe(Tp(4-NHCOC$_{10}$H$_{20}$SCOCH$_3$))(Tp)], has a gradual SCO with a $T_{½}$ of 366 K, consistent with literature reports on other molecules in the same family. The molecules retain their integrity and SCO properties in SAMs. ToF-SIMS, XPS semi-quantitative analyses, and PM-IRRAS confirm the presence of the molecule in the monolayers. The SAMs are of high quality: characterization by AFM indicates a homogeneous, uniform surface coverage; the PM-IRRAS indicates an ordered assembly with the expected thickness for a monolayer. The ordered packing is corroborated by CV, supported by DFT calculations, which indicates that each molecule occupies an area of 0.94 nm^2, consistent with the expected spherical diameter of the [FeTp$_2$] head group. Finally, XPS and XAS on the SAMs indicate a reversible SCO corresponding to the bulk behaviour, evidencing that we have successfully decoupled the SCO moiety from the metal substrates. Given their stability, robust SCO, and ability to form high quality monolayers, we expect that this family of molecules will bring promising results in the fields of molecular electronics and spintronics.

6. Experimental

Potassium tris(1H-pyrazol-1-yl borohydride) (≥97%) and 4-nitropyrazole (≥97%) were purchased from TCI. Tetrabutylammonium bromide (≥99%) and potassium thioacetate (≥98%) were purchased from Alfa Aesar. Anhydrous iron (II) chloride (≥98%), 10% palladium on carbon, thionyl chloride (≥99%), toluene (≥99.3%) and acetonitrile (≥99.9%) were purchased from Sigma Aldrich. 11-bromoundecanoic acid (≥ 99%) was purchased from Acros Organics. Acetonitrile was distilled over calcium hydride prior to use. Stabiliser-free, dry THF was obtained from an MBRAUN SPS 5 solvent purification system.

Synthesis of **FeTp$_2$-C11-SAc***: To obtain the [Fe(Tp-4-NH$_2$)(Tp)] and [Fe(Tp-4-NH$_2$)$_2$] building blocks, along with the non-functionalized [FeTp$_2$], we followed the synthesis described by Flötotto et. al..*[32] *We prepared 11-acetylthioundecanoyl chloride following the procedure described by Jaber et. al.,*[36] *and without exposing it to air we added the mixture of complexes (750 mg, 0.75 eq.) in dry THF then stirred in an ice bath for 2.5 h under argon. The resulting purple solid (888 mg) was purified first by size exclusion chromatography and then by silica gel chromatography, in toluene, to separate the bis-, mono- and non-functionalized complexes. The target molecule, the mono-substituted complex, is a pink sparkly powder. Attempts to obtain high quality single crystals for X-ray diffraction by evaporation or diffusion were unfortunately unsuccessful. The overall yield of these reaction steps, assuming a statistical 2:1:1 ratio of mono: bis: non-functionalized complex, is 15%. ^{1}H NMR (25°C, 400 MHz, benzene-d$_6$): δ 12.63 (m, 12H, Ar H), 9.80 (s, 1H, NH), 7.83 (3, 5H, Ar H), 2.82 (t, 2H, CH$_2$), 2.19 (t, 2H, CH$_2$), 2.11 (s, 3H, CH$_3$), 1.5 (m, 6H, CH$_2$), 1.24 (m, 10H, CH$_2$), -2.30 (s, 2H, BH); m/z: 739.5 (M, 100.00%), 740.3 (27.14), 738.5 (25.26), 741.4 (9.84), 737.5 (4.24), 742.4 (2.88), 743.3 (1.82), 745.3 (1.17), 736.6 (1.00), 744.3 (0.94); elemental analysis (% calcd, % found for C$_{31}$H$_{43}$B$_2$FeN$_{13}$O$_2$S, 739.29 gmol^{-1}): Fe (7.55, 6.66), B (2.92, 2.49), S (4.34, 4.20), C (50.36, 50.16), H (5.86, 6.05), N (24.63, 23.58).*

Mass spectrometry: MS analyses were performed on an LCQ Fleet Ion Trap (Thermo Fisher) spectrometer in direct injection mode in a 1:1 mixture of dichloromethane and methanol.

SAM preparation: the template stripped Au^{TS} substrates were prepared following standard procedure[44] *using a Korvus Technology HEX thermal evaporator to deposit the metals (200 nm) on a polished Si wafer,*

and Norland Optical Adhesive 61 to glue the glass substrates. The glass substrates and all glassware (vials and syringes) was thoroughly cleaned with Hellmanex III special cleaning concentrate and milliQ water. The SAMs were prepared by incubating the substrates in a solution of roughly 1 mg of ***FeTp$_2$-C11-SAc*** *in 3 mL of methanol, with a drop of triethylamine to deprotect the thioacetate, in a closed vial purged with argon. Upon removing the substrates from solution, the SAMs were rinsed with methanol and dried under a strong stream of nitrogen gas filtered through a 0.45 μm frit.*

VSM: Magnetic measurements on bulk FeTp$_2$-C11-SAc were performed in a Microsense EZ-7 vibrating sample magnetometer at a field strength of 1.5 T. FeTp$_2$-C11-SAc was weighed using a Mettler XPR2 ultramicrobalance and encapsulated in an light aluminium capsule for solids (Säntis). The magnetic contribution of the sample holder, measured independently on an empty capsule, fitted as a paramagnetic (Pauli) contribution together with a small Curie-like tail, was subtracted from the data, which was then corrected for sample diamagnetism using Pascal constants.

AFM: The surface morphology of the SAMs was characterized with a Bruker Dimension Fast Scan AFM in tapping mode, using NCHV antimony (n)-doped Si tips. The scan rate was 2 Hz on the Au substrate and 1 Hz on the SAM.

ToF-SIMS: The ToF-SIMS spectra were measured with a TOF.SIMS 5 spectrometer (IONTOF GmbH) equipped with a liquid metal ion gun (LMIG) oriented at 45° to the sample. The diameter of the LMIG 30 kV Bi_3^+ ion beam was approximatively 5 µm. The beam was operated at a 0.3 pA ion current in spectrometry mode and was raster scanned over the surface to generate 500 × 500 µm, 128 px × 128 px secondary ion images. Samples were grounded, and no charge effect was noticed during analysis. The total dose per image was kept below 10^8 ions cm^{-2}.

PM-IRRAS: The PM-IRRAS spectrum of the SAM of ***FeTp$_2$-C11-S*** *on gold was recorded on a ThermoNicolet Nexus 670 FTIR spectrometer at a resolution of 4 cm^{-1}, by coadding eight blocks of 1500 scans (4 h total acquisition time). All spectra were collected in a dry-air atmosphere. Experiments were performed at an incidence angle of 75° using an external homemade goniometer reflection attachment.*[71] *The infrared parallel beam (modulated in intensity at frequency f_i lower than 5 kHz) was directed out of the spectrometer with an optional flipper mirror and made slightly convergent with a first BaF_2 lens (191 mm focal length). The IR beam passed through a BaF_2 wire grid polarizer (Specac), to select the p-polarized radiation, and a ZnSe photoelastic modulator (PEM, Hinds Instruments, type II/ZS50). The PEM modulated the polarization of the beam at a high fixed frequency, $2f_m$=100 kHz, between the parallel and perpendicular linear states. After reflection on the sample, the double modulated (in intensity and in polarization) infrared beam was focused with a second ZnSe lens (38.1 mm focal length) onto a photovoltaic MCT detector (Kolmar Technologies, Model KV104) cooled at 77 K. The polarization modulated signal I_{AC} was separated from the low frequency signal I_{DC} (f_i between 500 and 5000 Hz) with a 40 kHz high pass filter and then demodulated with a lock-in amplifier (Stanford Model SR 830). The output time constant was set to 1 ms. The two interferograms were high-pass and low-pass filtered (Stanford Model SR 650) and simultaneously sampled in the dual channel electronics of the spectrometer. In all experiments, the PEM was adjusted for a maximum efficiency at 2500 cm^{-1} to cover the mid-IR range in only one spectrum. For calibration measurements, a second linear polarizer (oriented parallel or perpendicular to the first preceding the PEM) was inserted between the sample and the second ZnSe lens. This procedure was used to calibrate and convert the PM-IRRAS signal in terms of the IRRAS signal (i.e., $1 - R_p(d)/R_p(0)$) where $R_p(d)$ and $R_p(0)$ stand for the p-polarized reflectance of the film/substrate and bare substrate systems, respectively).*[72,73] *The polarized ATR spectra of* ***FeTp$_2$-C11-SAc*** *were recorded on a ThermoScientific iS50 FTIR spectrometer at a resolution of 4 cm^{-1}, by coadding 500 scans. ATR experiments were performed using a single-reflection ATR accessory (Specac) equipped with a germanium (Ge) crystal and a DTGS detector. A BaF_2 wire grid*

polarizer was added to record the spectra in the p- and s-polarizations. The film was obtained after successive evaporation of 10 µL of an ***FeTp$_2$-C11-SAc*** *chloroform solution dropped onto the Ge crystal.*

Electrochemistry: Cyclic voltammograms were recorded on a Methrom-AUTOLAB PGSTAT101 with a Pt counter electrode, Ag/AgCl pseudo reference electrode and either a Pt disk (1 mm^2) electrode (bulk measurement) or a patterned Au working electrode surface of 0.5 cm^2 which was incubated in the same working conditions as for the SAM measurement. The samples were measured in THF – 0.1 M NBu_4PF_6 and referenced to the Fc/Fc$^+$ redox couple, using a known quantity of ferrocene to determine the number of electrons transferred in the redox process. Measurements were done under inert atmosphere with constant nitrogen inflow.

DFT calculations: The geometry of the molecules was optimized by gas phase DFT calculations. The geometry was first pre-optimized using PM6 and was then further optimized by DFT with the B3LYP functional using the 6-31G(d,p) basis set as implemented in the Gaussian 09 program.[74]

XAS: Variable temperature XAS measurements were performed at the DEIMOS beamline[75–77] *at the SOLEIL synchrotron light source on the CROMAG endstation. X-ray absorption was measured in TEY mode under a 2 T magnetic field with circularly polarized incident X-rays using the HU-52 undulator. The temperature range was 4-350 K, the latter being the maximum attainable temperature in the CROMAG endstation. To prevent beam damage to the monolayer samples, a 50 µm aluminium filter was used and the monochromator was set up to ensure a photon density low enough to give less than 10 pA of signal from the sample. Under these conditions, no temporal evolution was observed during initial scans at 300 K. Eight spectra were measured at each temperature. These spectra were averaged and had a linear (given by a fit to the pre-edge region) and step background subtracted. A background contribution from the substrate,measured on bare Au^{TS}at each temperature, was also subtracted. The resulting spectra were normalized by the total integrated area in order to perform a quantitative fitting and analysis of the SCO.*

XPS: Variable temperature XPS measurements were performed using monochromatic Al Kα radiation ($h\nu$ = 1486.6 eV, SPECS mod. XR-MS focus 600) at a power of 100 W (13 kV, 7.7 mA) with a SPECS Phoibos 150 1-DLD electron analyser at 54.41° to the source. The fixed pass energy was 40 eV. A liquid nitrogen-based cryostat allowed for variable temperature measurements. The spectra were fit in CasaXPS after calibrating to the Fermi value of the gold substrate and removing the step background. The peaks were fit with 70/30 Voigt functions.

Supporting Information

Supporting Information is available from the Wiley Online Library or from the author.

Acknowledgements

The authors acknowledge the financial support from the Imperial College – CNRS joint PhD program, Quantum Matter Bordeaux, and the MaelStroM project (CNRS MITI program). The work was partially supported by MUR Italy through the program Dipartimenti di Eccellenza 2023-2027 (DICUS 2.0 grant, assigned to the Department of Chemistry “Ugo Schiff” of the University of Florence, CUP: B97G22000740001). The authors warmly thank C. Besson of Bingham University (U.S.A.) for her support and advice on chemical synthesis, J.P. Salvetat of the Placamat service unit (France) for the ToF-SIMS measurements, G. Pecastaings and X. Brilland of the Centre de Recherche Paul Pascal (France) for the AFM and MS measurements, N. Daro of the Chemical Analysis service at the ICMCB (France) for the CHNS and ICP measurements, the Magnetic Measurement service at the ICMCB for the VSM measurements, the

MatchLab Interdepartment Research Unit (Univ. of Florence), and the SOLEIL Synchrotron light source for beamtimes 20211046, 99210169, 20230820, 99240104 and for the support during XAS measurements.

Conflict of Interest

The authors declare no conflict of interest.

Data Availability Statement

The data that support the findings of this study are available from the corresponding authors upon reasonable request.

References

[1] D. Xiang, X. Wang, C. Jia, T. Lee, X. Guo, *Chem. Rev.* **2016**, *116*, 4318.
[2] G. Molnár, S. Rat, L. Salmon, W. Nicolazzi, A. Bousseksou, *Adv. Mater.* **2018**, *30*, 1703862.
[3] H. A. Goodwin, Philipp Gütlich, *Top Curr Chem* **2004**, *233*.
[4] H. Li, H. Peng, *Curr. Opin. Colloid Interface Sci.* **2018**, *35*, 9.
[5] M. Cinchetti, V. Alek Dediu, Luis E. Hueso, *Nat. Mater.* **2017**, *16*, 507.
[6] L. Poggini, M. Gonidec, J. H. González-Estefan, G. Pecastaings, B. Gobaut, P. Rosa, *Adv. Electron. Mater.* **2018**, *4*, 1800204.
[7] L. Poggini, M. Gonidec, R. K. Canjeevaram Balasubramanyam, L. Squillantini, G. Pecastaings, A. Caneschi, P. Rosa, *J. Mater. Chem. C* **2019**, *7*, 5343.
[8] S. K. Karuppannan, A. Martín-Rodríguez, E. Ruiz, P. Harding, D. J. Harding, X. Yu, A. Tadich, B. Cowie, D. Qi, C. A. Nijhuis, *Chem. Sci.* **2021**, *12*, 2381.
[9] T. G. Gopakumar, Matthias Bernien, Holger Naggert, Francesca Matino, Christian F. Hermanns, Alexander Bannwarth, Svenja Mühlenberend, Alex Krüger, Dennis Krüger, Fabian Nickel, Waldemar Walter, Richard Berndt, Wolfgang Kuch, Felix Tuczek, *Chem. Eur. J.* **2013**, *19*, 15702.
[10] S. Ossinger, H. Naggert, L. Kipgen, T. Jasper-Toennies, A. Rai, J. Rudnik, F. Nickel, L. M. Arruda, M. Bernien, W. Kuch, R. Berndt, F. Tuczek, *J. Phys. Chem. C* **2017**, *121*, 1210.
[11] S. Beniwal, X. Zhang, S. Mu, A. Naim, P. Rosa, G. Chastanet, J.-F. Létard, J. Liu, G. E. Sterbinsky, D. A. Arena, P. A. Dowben, A. Enders, *J. Phys. Condens. Matter* **2016**, *28*, 206002.
[12] M. Pénicaud, Incorporation of Spin Crossover Complexes in Molecular Electronics Devices, PhD Thesis, University of Bordeaux, **2023**.
[13] J. C. Love, L. A. Estroff, J. K. Kriebel, R. G. Nuzzo, G. M. Whitesides, *Chem. Rev.* **2005**, *105*, 1103.
[14] H. Naggert, A. Bannwarth, S. Chemnitz, T. Von Hofe, E. Quandt, F. Tuczek, *Dalton Trans.* **2011**, *40*, 6364.
[15] T. Mahfoud, G. Molnár, S. Cobo, L. Salmon, C. Thibault, C. Vieu, P. Demont, A. Bousseksou, *Appl. Phys. Lett.* **2011**, *99*, 053307.
[16] M. Gruber, R. Berndt, *Magnetochemistry* **2020**, *6*, 35.
[17] T. Miyamachi, M. Gruber, V. Davesne, M. Bowen, S. Boukari, L. Joly, F. Scheurer, G. Rogez, T. K. Yamada, P. Ohresser, E. Beaurepaire, W. Wulfhekel, *Nat. Commun.* **2012**, *3*, 938.
[18] A. Pronschinske, Y. Chen, G. F. Lewis, D. A. Shultz, A. Calzolari, M. Buongiorno Nardelli, D. B. Dougherty, *Nano Lett.* **2013**, *13*, 1429.
[19] M. Gruber, T. Miyamachi, V. Davesne, M. Bowen, S. Boukari, W. Wulfhekel, M. Alouani, E. Beaurepaire, *J. Chem. Phys.* **2017**, *146*, 092312.
[20] B. Warner, J. C. Oberg, T. G. Gill, F. El Hallak, C. F. Hirjibehedin, M. Serri, S. Heutz, M.-A. Arrio, P. Sainctavit, M. Mannini, G. Poneti, R. Sessoli, P. Rosa, *J. Phys. Chem. Lett.* **2013**, *4*, 1546.
[21] M. Pénicaud, E. Martinez, G. Serrano, B. Cortigiani, L. Squillantini, J. H. González-Estefan, E. Velez-Fort, M. Duttine, M. Gonidec, P. Rosa, M. Mannini, L. Poggini, *J. Mater. Chem. C* **2023**, *11*, 11518.
[22] E. J. Devid, P. N. Martinho, M. V. Kamalakar, I. Šalitroš, Ú. Prendergast, J.-F. Dayen, V. Meded, T. Lemma, R. González-Prieto, F. Evers, T. E. Keyes, M. Ruben, B. Doudin, S. J. Van Der Molen, *ACS Nano* **2015**, *9*, 4496.
[23] V. García-López, Niccolò Giaconi, Lorenzo Poggini, Amelie Juhin, Brunetto Cortigiani, Javier Herrero-Martín, Matteo Mannini, Miguel Clemente-León, Eugenio Coronado, *Adv. Funct. Mater.* **2023**, *33*, 2300351.
[24] L. Pukenas, F. Benn, E. Lovell, A. Santoro, L. J. Kershaw Cook, M. A. Halcrow, S. D. Evans, *J. Mater. Chem. C* **2015**, *3*, 7890.
[25] M. Gonidec, *Unpublished* **2024**.
[26] K. Bairagi, A. Bellec, C. Fourmental, O. Iasco, J. Lagoute, C. Chacon, Y. Girard, S. Rousset, F. Choueikani, E. Otero, P. Ohresser, P. Sainctavit, M.-L. Boillot, T. Mallah, V. Repain, *J. Phys. Chem. C* **2018**, *122*, 727.
[27] L. Zhang, Y. Tong, M. Kelai, A. Bellec, J. Lagoute, C. Chacon, Y. Girard, S. Rousset, M.-L. Boillot, E. Rivière, T. Mallah, E. Otero, M.-A. Arrio, P. Sainctavit, V. Repain, *Angew. Chem. Int. Ed.* **2020**, *59*, 13341.
[28] M. Kelai, V. Repain, A. Tauzin, W. Li, Y. Girard, J. Lagoute, S. Rousset, E. Otero, P. Sainctavit, M.-A. Arrio, M.-L. Boillot, T. Mallah, C. Enachescu, A. Bellec, *J. Phys. Chem. Lett.* **2021**, *12*, 6152.

[29] M. Kelai, A. Tauzin, A. Railean, V. Repain, J. Lagoute, Y. Girard, S. Rousset, E. Otero, T. Mallah, M.-L. Boillot, C. Enachescu, A. Bellec, *J. Phys. Chem. Lett.* **2023**, *14*, 1949.
[30] V. García-López, M. Palacios-Corella, V. Gironés-Pérez, C. Bartual-Murgui, J. A. Real, E. Pellegrin, J. Herrero-Martín, G. Aromí, M. Clemente-León, E. Coronado, *Inorg. Chem.* **2019**, *58*, 12199.
[31] N. Giaconi, A. L. Sorrentino, L. Poggini, G. Serrano, G. Cucinotta, E. Otero, D. Longo, H. Douib, F. Pointillart, A. Caneschi, R. Sessoli, M. Mannini, *Magnetochemistry* **2022**, *8*, 14.
[32] H. Flötotto, T. Secker, P. Kögerler, C. Besson, *Eur. J. Inorg. Chem.* **2019**, *2019*, 4621.
[33] C. E. D. Chidsey, C. R. Bertozzi, T. M. Putvinski, A. M. Mujsce, *J. Am. Chem. Soc.* **1990**, *112*, 4301.
[34] T. Auletta, F. C. J. M. Van Veggel, D. N. Reinhoudt, *Langmuir* **2002**, *18*, 1288.
[35] C. A. Nijhuis, W. F. Reus, G. M. Whitesides, *J. Am. Chem. Soc.* **2009**, *131*, 17814.
[36] N. Jaber, A. Lesniewski, H. Gabizon, S. Shenawi, D. Mandler, J. Almog, *Angew. Chem. Int. Ed.* **2012**, *51*, 12224.
[37] E. Becker, S. Pavlik, K. Kirchner, *Adv. Organomet. Chem.* **2008**, *56*, 156.
[38] C. Ma, C. Besson, *Dalton Trans.* **2021**, *50*, 18077.
[39] M. Baskin, N. Fridman, M. Kosa, G. Maayan, *Dalton Trans.* **2017**, *46*, 15330.
[40] I. Nikovskiy, D. Yu. Aleshin, V. V. Novikov, A. V. Polezhaev, E. A. Khakina, E. K. Melnikova, Y. V. Nelyubina, *Inorg. Chem.* **2022**, *61*, 20866.
[41] B. Hutchinson, L. Daniels, E. Henderson, P. Neill, G. J. Long, L. W. Becker, **1979**.
[42] F. Grandjean, G. J. Long, B. B. Hutchinson, L. Ohlhausen, P. Neill, J. D. Holcomb, *Inorg. Chem.* **1989**, *28*, 4406.
[43] L. Salmon, G. Molnár, S. Cobo, P. Oulié, M. Etienne, T. Mahfoud, P. Demont, A. Eguchi, H. Watanabe, K. Tanaka, A. Bousseksou, *New J. Chem.* **2009**, *33*, 1283.
[44] N. Vogel, J. Zieleniecki, I. Köper, *Nanoscale* **2012**, *4*, 3820.
[45] M. P. Gil, J. H. Z. dos Santos, O. L. Casagrande Jr., *Macromol Chem Phys* **2001**, 319.
[46] K. Heister, M. Zharnikov, M. Grunze, L. S. O. Johansson, A. Ulman, *Langmuir* **2001**, *17*, 8.
[47] C. Shen, M. Haryono, A. Grohmann, M. Buck, T. Weidner, N. Ballav, M. Zharnikov, *Langmuir* **2008**, *24*, 12883.
[48] D. D. Popenoe, S. M. Stole, M. D. Porter, *Appl. Spectrosc.* **1992**, *46*, 79.
[49] L. Sang, A. Mudalige, A. K. Sigdel, A. J. Giordano, S. R. Marder, J. J. Berry, J. E. Pemberton, *Langmuir* **2015**, *31*, 5603.
[50] V. Jangid, D. Brunel, E. Sanchez-Adaime, A. K. Bharwal, F. Dumur, D. Duché, M. Abel, M. Koudia, T. Buffeteau, C. A. Nijhuis, G. Berginc, C. Lebouin, L. Escoubas, *Langmuir* **2022**, *38*, 3585.
[51] A. T. Hubbard, F. C. Anson, A. J. Bard, *Electroanalytlcal Chemistry*, Marcel Dekker, New York, **1970**.
[52] A. J. Bard, L. R. Faulkner, H. S. White, *Electrochemical Methods: Fundamentals and Applications*, Wiley & Sons, **2002**.
[53] A. L. Eckermann, D. J. Feld, J. A. Shaw, T. J. Meade, *Coord. Chem. Rev.* **2010**, *254*, 1769.
[54] E. Laviron, *J Electroanal Chem* **1979**, 263.
[55] K. Takehara, H. Takemura, Y. Ide, *Electrochimica Acta* **1994**, *39*, 817.
[56] L. Y. S. Lee, T. C. Sutherland, S. Rucareanu, R. B. Lennox, *Langmuir* **2006**, *22*, 4438.
[57] E. C. Ellingsworth, B. Turner, G. Szulczewski, *RSC Adv.* **2013**, *3*, 3745.
[58] M. Atzori, L. Poggini, L. Squillantini, B. Cortigiani, M. Gonidec, P. Bencok, R. Sessoli, M. Mannini, *J. Mater. Chem. C* **2018**, *6*, 8885.
[59] L. Poggini, M. Milek, G. Londi, A. Naim, G. Poneti, L. Squillantini, A. Magnani, F. Totti, P. Rosa, M. M. Khusniyarov, M. Mannini, *Mater. Horiz.* **2018**, *5*, 506.
[60] L. Poggini, G. Londi, M. Milek, A. Naim, V. Lanzilotto, B. Cortigiani, F. Bondino, E. Magnano, E. Otero, P. Sainctavit, M.-A. Arrio, A. Juhin, M. Marchivie, M. M. Khusniyarov, F. Totti, P. Rosa, M. Mannini, *Nanoscale* **2019**, *11*, 20006.
[61] L. N. Mazalov, I. P. Asanov, V. A. Varnek, *J. Electron Spectrosc. Relat. Phenom.* **1998**, *96*, 209.
[62] K. Burger, C. Furlani, G. Mattogno, *J. Electron Spectrosc. Relat. Phenom.* **1980**, 249.
[63] J. Matienzo, L. I. Yin, S. O. Grim, W. E. Swartz, *Inorg. Chem.* **1973**, *12*, 2762.
[64] C. Cartier Dit Moulin, P. Rudolf, A. M. Flank, C. T. Chen, *J. Phys. Chem.* **1992**, *96*, 6196.
[65] D. Collison, C. D. Garner, C. M. McGrath, J. F. W. Mosselmans, M. D. Roper, J. M. W. Seddon, E. Sinn, N. A. Young, *J. Chem. Soc. Dalton Trans.* **1997**, 4371.

[66] J.-J. Lee, H. Sheu, C.-R. Lee, J.-M. Chen, J.-F. Lee, C.-C. Wang, C.-H. Huang, Y. Wang, *J. Am. Chem. Soc.* **2000**, *122*, 5742.
[67] M.-A. Arrio, Ph. Sainctavit, Ch. Cartier Dit Moulin, Ch. Brouder, F. M. F. De Groot, T. Mallah, M. Verdaguer, *J. Phys. Chem.* **1996**, *100*, 4679.
[68] B. T. Thole, G. Van Der Laan, *Phys. Rev. B* **1988**, *38*, 3158.
[69] G. V. D. Laan, I. W. Kirkman, *J. Phys. Condens. Matter* **1992**, *4*, 4189.
[70] P. Totaro, L. Poggini, A. Favre, M. Mannini, P. Sainctavit, A. Cornia, A. Magnani, R. Sessoli, *Langmuir* **2014**, *30*, 8645.
[71] T. Buffeteau, B. Desbat, J. M. Turlet, *Appl. Spectrosc.* **1991**, *45*, 380.
[72] T. Buffeteau, B. Desbat, D. Blaudez, J. M. Turlet, *Appl. Spectrosc.* **2000**, *54*, 1646.
[73] M. A. Ramin, G. Le Bourdon, N. Daugey, B. Bennetau, L. Vellutini, T. Buffeteau, *Langmuir* **2011**, *27*, 6076.
[74] M. J. Frisch, G. W. Trucks, J. R. Cheeseman, G. Scalmani, M. Caricato, H. P. Hratchian, X. Li, V. Barone, J. Bloino, G. Zheng, T. Vreven, J. A. Montgomery, G. A. Petersson, G. E. Scuseria, H. B. Schlegel, H. Nakatsuji, A. F. Izmaylov, R. L. Martin, J. L. Sonnenberg, J. E. Peralta, J. J. Heyd, E. Brothers, F. Ogliaro, M. Bearpark, M. A. Robb, B. Mennucci, K. N. Kudin, V. N. Staroverov, R. Kobayashi, J. Normand, A. Rendell, R. Gomperts, V. G. Zakrzewski, M. Hada, M. Ehara, K. Toyota, R. Fukuda, J. Hasegawa, M. Ishida, T. Nakajima, Y. Honda, O. Kitao, H. Nakai, *Gaussian 09 Version A02* **2009**, *Gaussian, Inc., Wallingford CT*.
[75] P. Ohresser, E. Otero, F. Choueikani, K. Chen, S. Stanescu, F. Deschamps, T. Moreno, F. Polack, B. Lagarde, J.-P. Daguerre, F. Marteau, F. Scheurer, L. Joly, J.-P. Kappler, B. Muller, O. Bunau, Ph. Sainctavit, *Rev. Sci. Instrum.* **2014**, *85*, 013106.
[76] L. Joly, E. Otero, F. Choueikani, F. Marteau, L. Chapuis, P. Ohresser, *J. Synchrotron Radiat.* **2014**, *21*, 502.
[77] J.-P. Kappler, E. Otero, W. Li, L. Joly, G. Schmerber, B. Muller, F. Scheurer, F. Leduc, B. Gobaut, L. Poggini, G. Serrano, F. Choueikani, E. Lhotel, A. Cornia, R. Sessoli, M. Mannini, M.-A. Arrio, Ph. Sainctavit, P. Ohresser, *J. Synchrotron Radiat.* **2018**, *25*, 1727.

Table of Contents Entry

The table of contents entry should be 50–60 words long and should be written in the present tense. The text should be different from the abstract text. Impersonal style. For general audience.

Rebecca Rodrigues de Miranda, Niccolò Giaconi, Margaux Pénicaud, Lisa Biwandu, Thierry Buffeteau, Brunetto Cortigiani, Matteo Mannini, Edwige Otero, Philippe Ohresser, Elizabeth Hillard, Lorenzo Poggini, Mathieu Gonidec,* Patrick Rosa**

Non-Pinned, Reversible Spin Crossover in Self-Assembled Monolayers of a Functionalized Fe(II) Scorpionate Complex

ToC figure ((Please choose one size: 55 mm broad × 50 mm high **or** 110 mm broad × 20 mm high. Please do not use any other dimensions)). Should convey main message of article